Chin. Phys. Lett. **39**, 068501 (2022)

Indium-Gallium-Zinc-Oxide-Based Photoelectric Neuromorphic Transistors for Spiking Morse Coding

Xinhuang Lin(林鑫煌), Haotian Long(龙昊天), Shuo Ke(柯硕), Yuyuan Wang(王宇远), Ying Zhu(祝影), Chunsheng Chen(陈春生), Changjin Wan(万昌锦)*, and Qing Wan(万青)*

School of Electronic Science and Engineering, Nanjing University, Nanjing 210093, China

(Received 28 March 2022; accepted 25 April 2022; published online 29 May 2022)

The human brain that relies on neural networks communicated by spikes is featured with ultralow energy consumption, which is more robust and adaptive than any digital system. Inspired by the spiking framework of the brain, spike-based neuromorphic systems have recently inspired intensive attention. Therefore, neuromorphic devices with spike-based synaptic functions are considered as the first step toward this aim. Photoelectric neuromorphic devices are promising candidates for spike-based synaptic devices with low latency, broad bandwidth, and superior parallelism. Here, the indium-gallium-zinc-oxide-based photoelectric neuromorphic transistors are fabricated for Morse coding based on spike processing, 405-nm light spikes are used as synaptic inputs, and some essential synaptic plasticity, including excitatory postsynaptic current, short-term plasticity, and high-pass filtering, can be mimicked. More interestingly, Morse codes encoded by light spikes are decoded using our devices and translated into amplitudes. Furthermore, such devices are compatible with standard integrated processes suitable for large-scale integrated neuromorphic systems.

DOI: 10.1088/0256-307X/39/6/068501

Inspired by spiking neural networks in the human brain, neuromorphic systems enable the brain-like efficient and parallel information processing.[1–3] Such systems can realize efficient artificial intelligence while reducing the computational load and energy of the computing platform.[4–9] Therefore, the hardware implementation of neuromorphic systems with spike-encoding capability has increasingly attracted attention.[10–12] An essential component of such hardware is the photoelectric synapse with adjustable conductance weight.[13,14] Photoelectric synapses have been developed to simulate spike-based synaptic functions capable of detecting and integrating the light spikes into an excitatory postsynaptic current (EPSC).[15–17] Additionally, indium-gallium-zinc-oxide (IGZO)-based photoelectric neuromorphic synapses use light spikes as external synaptic inputs, indicating high potential for next-generation neuromorphic systems due to their excellent properties such as low latency, broad bandwidth, and superior parallelism.[18–20]

So far, artificial synapses based on photoelectric neuromorphic devices with simple spike-driven applications have been reported. In 2020, Tan *et al.*[21] reported that a photoelectric spike afferent neuron with perceptual learning and neural coding simulates tactile processing and perception. Inspired by the brain, the photoelectric synapse with synaptic coding through spike-driven processing has significant prospects for efficient intelligence applications.

In this Letter, IGZO thin-film transistors (TFTs) are used for operating photoelectric neuromorphic synapses. The light spikes are the wireless communication medium for loading information. The synaptic information transmission is emulated based on the spikes' processing. Moreover, the devices are used as a real-time decoder that translates the Morse coding sequence into the EPSC amplitudes. Such devices are compatible with the standard integrated processes, providing opportunities for expanding the application of large-scale integrated photoelectric neuromorphic systems.

The inset of Fig. 1(c) illustrates the bottom gate structure of the IGZO-based photoelectric neuromorphic transistors. The semiconductor channel and source/drain electrodes were both patterned using photolithography. First, the Al_2O_3 gate dielectric film was deposited on a heavily doped n-type silicon substrate (with $Si(N^+)$ as the gate electrode) at 120 ℃ with a thickness of ∼20 nm by atomic layer deposition. Second, after the first photolithography process, the IGZO film (In : Ga : Zn = 2 : 2 : 1, 40 nm) was deposited using RF magnetron sputtering and patterned by a liftoff process. During the sputtering process, the power density, the working pressure, and the O_2/Ar mixture flow rate were 4.9 W/cm^2, 0.5 Pa, and 1.6/30 sccm, respectively. Next, the IGZO film was annealed at 350 ℃ for 1 h under ambient air to improve the channel's quality.[22,23] Finally, after the second photolithography process, 200-nm-thick

*Corresponding authors. Email: wanqing@nju.edu.cn; cjwan@nju.edu.cn
© 2022 Chinese Physical Society and IOP Publishing Ltd

Al source and drain electrodes were deposited using the thermal evaporation method and patterned using a liftoff process. Figure 1(a) shows the overhead view of the optical microscopy image. The effective length and width of the IGZO channel measure about 2.17 and 19.64 µm, respectively. A fiber-coupled laser module (Changchun New Industries Laser PGL-FC-405 nm) was used to apply 405-nm light spikes to the IGZO channel. A semiconductor parameter analyzer (KEITHLEY 2636B) was employed to investigate the electrical characteristics of the neuromorphic device. All measurements were performed at room temperature.

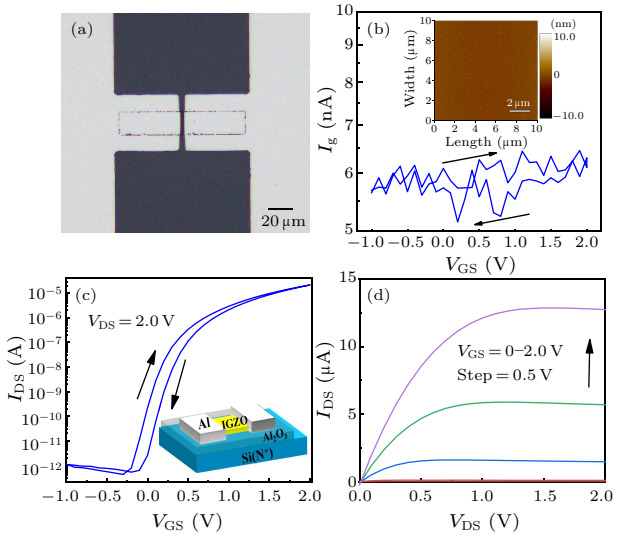

Fig. 1. (a) Overhead view of the optical microscopy image for IGZO-based photoelectric neuromorphic transistors. (b) Devices' gate leakage curve (I_g versus V_{GS}). Inset: AFM image of the IGZO channel. (c) Devices' transfer curve (I_{DS} versus V_{GS}) with V_{DS} fixed at 2.0 V. Inset: Structure of the IGZO-based photoelectric neuromorphic transistors. (d) Devices' output curve (I_{DS} versus V_{DS}) with V_{DS} from 0 to 2.0 V at a 0.5 V step.

The fundamental characteristics of the devices are present. The inset of Fig. 1(b) displays an AFM image of the IGZO channel. The root-mean-square surface roughness is as low as 0.525 nm. Figure 1(b) shows the gate leakage current of the devices. A maximum leakage current of ∼6.44 nA at 2.0 V was obtained. A smooth channel surface and low leakage current are favorable for the charge carrier transport in semiconductor channel, which also improve the devices' comprehensive performance.[24,25] Figure 1(c) shows the transfer curve (I_{DS} versus V_{GS}) of the device with V_{DS} fixed at 2.0 V. During the model of reverse V_{GS} scanning, the I_{DS} can be effectively modulated, and a clockwise hysteresis loop of ∼0.2 V can be obtained, possibly due to the electron trapping near the IGZO/Al_2O_3 interface or within the IGZO channel film.[26] A high channel current ON/OFF ration (I_{ON}/I_{OFF}) is estimated to be 5.2×10^7. The threshold voltage (V_{TH}) is about 0.41 V obtained from the X-axis intercept on the $I_{DS}^{1/2}$–V_G plot. The subthreshold swing value is as low as ∼105 mV/dec, representing the gate voltage required for an order of decade I_{DS} increasing. The field-effect mobility (μ_{FE}) of ∼6.48 $cm^2 \cdot V^{-1} \cdot s^{-1}$ in the saturation region is extracted from the relation equation $I_{DS} = \mu W C_i (V_{GS} - V_{TH})^2/2L$, where L and W are the effective channel length and width, respectively, and C_i is the specific capacitance of the Al_2O_3 gate dielectric (estimated to be 0.294 µF·cm^{-2} at 1.0 Hz). Meanwhile, Fig. 1(d) shows the device's output curve (I_{DS} versus V_{DS}) with V_{DS} from 0 to 2.0 V in steps of 0.5 V. This shows that the ohmic contact is formed at the channel–electrode interface, indicating significant n-type channel TFT characteristics and high performance in pinch and saturation characteristics. The maximum channel current measured is 12.75 µA in the saturation region under V_{GS} = 2.0 V and V_{DS} = 2.0 V. The transfer and output curve show the high performance of devices, providing a good foundation for realizing the Morse code application.

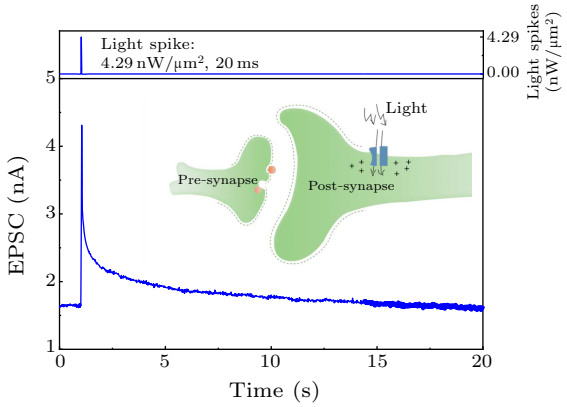

Fig. 2. A sharp response EPSC can be observed immediately when a light spike stimulates the device. Inset: The action potential changes induced by the difference in ion concentration between the two sides of the biological synapse membrane.

In this study, the light spikes are applied to the IGZO channel and used as the communication medium for loading information. Additionally, the intensity and width of the 405-nm light spikes are 4.29 nW/$µm^2$ and 20 ms, respectively, and the V_{DS} at a fixed value of 0.1 V with V_{GS} = 0 V. When 405-nm light spikes stimulate the devices, the light-induced electrons are generated in the semiconductor channel, increasing the conductivity. This is known as the photoconductivity effect.[27] The photo-generated electrons will be constantly recaptured to the trap sites when the light spike stimuli are turned off. Short-term plasticity (STP) can be achieved by applying few repeated light stimuli that cause a short recombination time of photogenerated electrons.[13] In our neuromorphic devices, the channel photocurrent is the EPSC to emulate the spike-based information trans-

mission in the synapse. As shown in Fig. 2, a sharp response EPSC is induced between the source and drain, which then declines rapidly to the original current state, mimicking the STP characteristics. In the biological systems, the external stimuli with environmental information are encoded with action potentials (named spikes), which are conveyed to the central nervous system through synapses.[28] As shown in the inset of Fig. 2, the EPSC occurring in the IGZO channel is similar to the action potential induced by the ion concentration difference between the two sides of the biologicalsynapse membrane.[29] Using light spikes as the stimulation source shows that the basic biosynaptic function, including spike-based information transmission, can be mimicked in our devices.

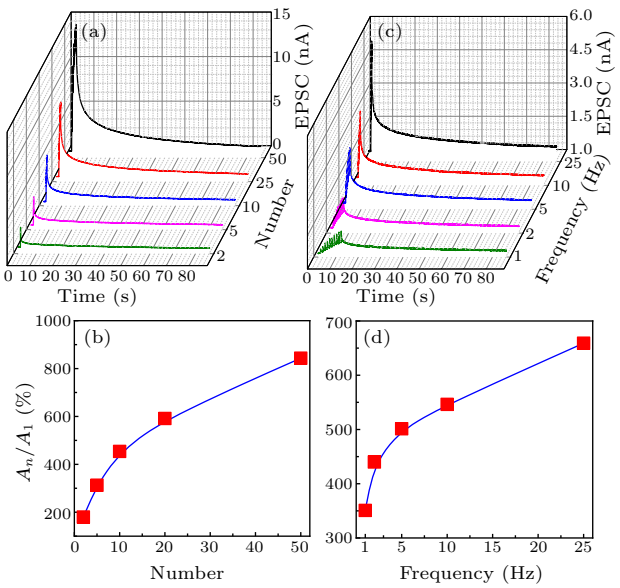

Fig. 3. (a) EPSC induced by different number of light spikes. (b) The value of A_n/A_1 at different numbers of light spikes. (c) EPSC amplitude induced by different frequencies of light spikes. (d) The value of A_n/A_1 at different frequencies of light spikes.

If the amplitude of the EPSC induced by the external light spikes can be controlled, the IGZO-based photoelectric neuromorphic synapses can effectively decode the environmental information. Two test plans with different light spike frequencies are designed to study the spiking modulation process. Figure 3(a) shows that the amplitude of the EPSC increases rapidly with an increase in the number of light spikes. A_n/A_1 is defined as the ratio of the amplitude gain between the EPSC induced by the nth light spike and the EPSC induced by the first light spike. As shown in Fig. 3(b), the value of A_n/A_1 is 180% at the beginning at two light spikes and increases to 843% at the end at 50 light spikes. It was observed that the channel weight conductance increases with an increase in the number of light spikes. This gradual transformation from weak to strong mimics the biological synapse's facilitation behavior and learning process.[30] As shown in Fig. 3(c), the amplitude of the EPSC increases rapidly by increasing the light spike frequency. As shown in Fig. 3(d), the value of A_n/A_1 is 350% at the beginning of 1 Hz and increases to 659% at the end of 25 Hz. A_n/A_1 increases rapidly with an increase in frequency, indicating the dynamic high-pass filtering, namely, the stronger coupling between the light spikes at higher frequency.[31,32] Such a phenomenon shows that the EPSC amplitudes are controlled efficiently based on the spiking modulation process. Therefore, for spiking the Morse code application, photoelectric neuromorphic transistors can effectively decode the environmental information and translate it into amplitudes.

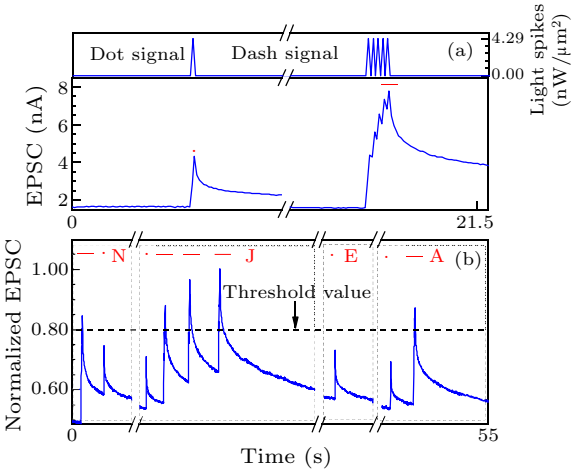

Fig. 4. (a) The dot light spike (25 ms, 1 spike) and dash light spikes (25 ms, 25 Hz with 5 spikes) are as dot signal and dash signal in the Morse code, respectively. (b) Recognition of the word "NJEA", which encodes into light spikes with the Morse code. The devices are used as decoder with the spikes encoding, and the threshold value of the normalized EPSC is set as 0.80.

The Morse code is the most common method of transmitting information through temporal series.[33] It uses specific order to show different letters, numbers, and punctuation marks. The dot (·) and dash (−) signals are the basic signals in the Morse code. In this work, the light spikes are the wireless medium for loading information in the temporal coding sequence. The photoelectric neuromorphic transistors are used as decoders for the information encoded with the light spikes. As shown in Fig. 4(a), the dot light spike (20 ms, 1 spike) and dash light spikes (20 ms, 25 Hz with 5 spikes) serve as dot and dash input signals, respectively. When the Morse code characters are read, the photoelectric neuromorphic transistors produce EPSC signals composed of several spikes. By distinguishing the amplitude of every response spike, the devices can decode the dot and dash signals. As shown in Fig. 4(b), under considerable interval time between every input signal, the short word "NJEA" is encoded with the Morse code into the external light spikes and

decoded by the IGZO-based photoelectric synapses. The threshold value of the normalized EPSC to distinguish the input signal between the dot and dash signals is set as 0.80. The normalized value is defined as the EPSC divided by the maximum value of the EPSC in the measurement. It is clear that the devices used as decoders use the amplitude of the response signal to recognize each letter accurately. These results show that such photoelectric devices can realize communication applications when using light spikes as the wireless medium. Consequently, the neuromorphic transistors are used as real-time photoelectric decoders for spiking the Morse coding, providing the possibility of performing efficient communication as a part of the photonic neuromorphic systems.

In summary, IGZO-based photoelectric neuromorphic transistors have been fabricated for spike-encoding applications. The amplitudes of the EPSC induced by the photoelectric neuromorphic transistors are effectively modulated using the light spikes. Moreover, the devices are used as decoders for light information encoded by the Morse code. With the implementation of the spiking coding based on the EPSC amplitude modulation, such photoelectric neuromorphic devices have significant prospects for developing light wireless communication, smart photoelectronic prostheses, and artificial vision systems. Furthermore, our devices are compatible with the standardized integrated process, promising a strategy for large-scale integrated photonic neuromorphic systems.

Acknowledgments. This work was supported by the National Key Research and Development Program of China (Grant No. 2019YFB2205400), and the National Natural Science Foundation of China (Grant No. 62074075).

References

[1] van de Burgt Y, Melianas A, Keene S T, Malliaras G *et al.* 2018 *Nat. Electron.* **1** 386
[2] Li Y, Yin K, Diao Y, Fang M *et al.* 2022 *Nanoscale* **14** 2316
[3] Park Y and Lee J S 2017 *ACS Nano* **11** 8962
[4] Liao F, Zhou Z, Kim B J, Chen J *et al.* 2022 *Nat. Electron.* **5** 84
[5] Deco G, Rolls E T and Romo R 2009 *Prog. Neurobiol.* **88** 1
[6] He Y, Nie S, Liu R, Jiang S *et al.* 2018 *J. Mater. Chem. C* **6** 5336
[7] John R A, Liu F, Chien N A, Kulkarni M R *et al.* 2018 *Adv. Mater.* **30** 1800220
[8] Kim M K, Park Y, Kim I J and Lee J S 2020 *iScience* **23** 101846
[9] Marković D, Mizrahi A, Querlioz D and Grollier J 2020 *Nat. Rev. Phys.* **2** 499
[10] Sheridan P M, Cai F, Du C, Ma W *et al.* 2017 *Nat. Nanotechnol.* **12** 784
[11] Roy K, Jaiswal A and Panda P 2019 *Nature* **575** 607
[12] Yang J Q, Wang R, Ren Y, Mao J Y *et al.* 2020 *Adv. Mater.* **32** 2003610
[13] Zhou F, Zhou Z, Chen J, Choy T H *et al.* 2019 *Nat. Nanotechnol.* **14** 776
[14] Zhang J, Dai S, Zhao Y W, Zhang J H *et al.* 2020 *Adv. Intell. Syst.* **2** 1900136
[15] Li H K, Chen T P, Liu P, Hu S G *et al.* 2016 *J. Appl. Phys.* **119** 244505
[16] Dai S, Wu X, Liu D, Chu Y *et al.* 2018 *ACS Appl. Mater. Interfaces* **10** 21472
[17] Seo S, Jo S H, Kim S, Shim J *et al.* 2018 *Nat. Commun.* **9** 5106
[18] Zhu L, He Y, Chen C, Zhu Y *et al.* 2021 *IEEE Trans. Electron. Devices* **68** 1659
[19] Song S, Kim J, Kwon S M, Jo J W *et al.* 2021 *Adv. Intell. Syst.* **3** 2000119
[20] Shastri B J, Tait A N, de Ferreira L T, Pernice W H P *et al.* 2021 *Nat. Photon.* **15** 102
[21] Tan H, Tao Q, Pande I, Majumdar S *et al.* 2020 *Nat. Commun.* **11** 1369
[22] Qin G P, Zhang H, Ruan H B, Wang J *et al.* 2019 *Chin. Phys. Lett.* **36** 047301
[23] Lee E, Kim T H, Lee S W, Kim J H *et al.* 2019 *Nano Converg.* **6** 24
[24] Lee C Y, Joo Y H, Kim M P, Um D S *et al.* 2021 *Coatings* **11** 906
[25] Ma P F, Du L L, Wang Y M, Jiang R *et al.* 2018 *Appl. Phys. Lett.* **112** 023501
[26] He Y, Nie S, Liu R, Jiang S *et al.* 2019 *IEEE Electron Device Lett.* **40** 818
[27] Yoo H, Lee I S, Jung S, Rho S M *et al.* 2021 *Adv. Mater.* **33** 2006091
[28] Abraira V E and Ginty D D 2013 *Neuron* **79** 618
[29] Kim M K and Lee J S 2020 *Adv. Mater.* **32** 1907826
[30] Gao S, Liu G, Yang H, Hu C *et al.* 2019 *ACS Nano* **13** 2634
[31] Zhao Y, Liu B, Yang J, He J *et al.* 2020 *Chin. Phys. Lett.* **37** 088501
[32] Nie S, He Y L, Liu R, Shi Y *et al.* 2019 *IEEE Electron Device Lett.* **40** 459
[33] Yang C H 2000 *Med. Eng. Phys.* **22** 59